STUDY OF STRUCTURAL, OPTICAL AND ELECTRICAL PROPERTIES OF FLUORINE, COBALT DOPED AND FLUORINE-COBALT CO-DOPED TIN DIOXIDE SnO_2

M. MAHMOUDI[a,b,c*], A. BENHAOUA[c,d], B. BENHAOUA[d], L. SEGUENI[b], R. GHERIANI[a,c], A. RAHAL[c,d]

[a]*Faculty of Mathematics and Material Sciences, Univ. Ouargla, Ouargla 30000, Algeria*
[b]*Lab. VTRS, Faculty of Science & Technology, Univ. El-Oued, El Oued 39000, Algeria*
[c]*Lab. LRPPS, UKM Ouargla 30000, Algeria*
[d]*Unité de Développement des Energies Renouvelables dans les Zones Arides (UDERZA), Univ. El-Oued, El Oued 39000, Algeria*

In this study, undoped, fluorine, cobalt and fluorine-cobalt co-doped tin dioxide SnO_2 thin films have been deposited onto 480°C preheated glass substrates using the spray pyrolysis technique with moving nozzle (SPMN). Structural and opto-electrical properties of undoped tin oxide and F/Co and F-Co co-doped SnO_2 tin films were investigated. The used sources for SnO_2 product and its doping F, and Co elements are $SnCl_2$, NH4F and $CoCl_2$, respectively. The studied samples are 7 wt % F/Sn, 2.5 wt % Co/Sn, and (7 wt% F/Sn +2.5 wt% Co/Sn) co-doped SnO_2. Effect of F doping , Co doping and co-dopeding concentration on structural and optical properties of SnO_2 thin films was investigated. Structural studies using X-ray diffraction show that formation of SnO_2 under rutile structure with several diffraction peaks at 2θ = 37.95, 26.61 and 51.82°along (200), (110) and (211) planes, respectively. Further the more peak at 29.9° corresponding to (101) plan of SnO phase formation was observed only with F-doping and Co-doping SnO_2 cases. (200) peak intensity increases to reach its maximum with Co-doped SnO_2 becomes more significant, when F/Co reaches 0.1M, leading to an increment in SnO_2 crystallite size over 23.33nm for the considered concentration. FT-IR analysis of spectra confirmed the existence of Sn-O, F-Sn-F, and Sn-F bonds vibrations modes in the product. UV-visible investigation of optical transmittance spectra showed that the films have transparence ranged in 73-83% and fluctuated band gap energy in the average 3.77 to 3.94eV whereas the films thicknesses varied between 960-1373nm.

(Received July 22, 2019; Accepted November 29, 2019)

Keywords: Thin films, F-Co co-doped SnO_2, Spray pyrolysis, Optical properties, FT-IR

1. Introduction

Transparent conducting oxides (TCOs) thin films are very useful materials for many applications. They have a wide use in solar cells, optoelectronics and display devices, catalytic, heat mirrors smart window and so on [1-5]. Among them, doped tin oxide (SnO_2) is of particular employ because of its owing important properties which are the good electrical conductivity and high transparency in the visible region. Such properties make it an ideal candidate for others application more than cited above. SnO_2 thin films are prepared by many techniques: chemical vapor deposition [6], sputtering[7], sol-gel [8, 9], reactive evaporation [10], pulsed laser ablation [11], photochemical method [12], ultrasonic spray method and spray pyrolysis [13, 14]. Among these deposition techniques spray pyrolysis which is a simple low cost method for great area coating.[15] Fluorine (F), iron (Fe), antimony (Sb), molybdenum (Mo), indium (In), palladium (Pd), cerium (Ce), niobium (Nb), and cobalt (Co) doping were achieved to improve tin oxide (SnO_2) properties[16-22]. Among those dopants fluorine and cobalt co-doped tin oxide are few studied.

* Corresponding author: manelmahmoudi2012@gmail.com

In the research, elaboration of F, Co doped tin dioxide (FTO), (CTO), and F-Co co-doped tin dioxide (FCTO) transparent conducting thin films on glass slides will be achieved. $SnCl_2$, NH_4F and $CoCl_2$ have been used as sources of Sn, F, and Co elements, respectively, to prepare undoped tin dioxide (SnO_2), (FTO), (CTO), and (FCTO) thin films. The later have been sprayed via pyrolysis technique with moving nozzle (SPMN) [23] Investigation of their physical properties will be undergone using structural, optical, and electrical apparatus equipment.

2. Experimental details

2.1. Preparation of (SnO_2), (FTO), (CTO), and (FCTO) thin films

Undoped, F doped, Co doped and F-Co co-doped tin oxide thin films were elaborated using tin chloride dehydrate ($SnCl_2$, $2H_2O$), ammonium fluoride (NH_4F) and cobalt chloride dehydrate ($CoCl_2$, $6H_2O$) as sources of Sn, F, and Co elements, respectively. The sources were dissolved in double distilled water and methanol in volume ratio (1/2:1/2) in respect of theoretical amounts of doping 7wt.% F doped SnO_2; 2.5wt.% Co doped SnO_2, 7wt.% F+2.5 wt.% Co co-doped SnO_2. The obtained solutions were sprayed onto 480°C heated glass substrates (Ref 217102: having 7.5x2.5x0.13cm^3 as dimensions) with keeping distance nozzle-substrate equal to 5cm; whereas the deposition time was 5min with spray rate of 5ml/min. The moving nozzle was used to save the stability of substrate temperature.

2.2. Characterization

The optical transmittance and FT-IR absorbance measurements were recorded in the spectral region of (200-900nm) and (400-4500cm^{-1}) by using UV-visible spectrophotometer (Shimadzu, Model 1800) and (Shimadzu, IR Affinity-1), respectively. The structural characterization of the achieved thin films was carried out, on 1×1 cm^2 sample sheets, by X-ray diffraction (XRD) with an X-ray diffractometer (BRUKER-AXS type D8) equipped with X'Pert High Score under Cu Ka (l = 1.5405Å) radiation whereas the scanning range of (2θ) was between 10-90°. Morphology survey of the films is done by the scanning electron micrographs (SEM). The measurements were conducted at room temperature (rt). Sheet resistance evaluation was measured via four-point probe technique on 1x1 cm^2 samples sheets.

3. Results and discussion

3.1. Optical properties

The transmittance spectra of the samples are shown in Fig. 1. For all of them, the average transmittance was taken at 450, 600, 750nm, respectively which was found more than 78, 77, 73 and 83% for undoped, F-doped, Co-doped and F+Co co-doped SnO_2, respectively. It means that in the visible region, the films show an increase in transmittance after (F, Co) doping separately and more enhanced for the co-doped. Due to the existence of interference fringes and in respect to Manifacier and Swanepoel formula [24], the calculated thickness (t) of the layers was done as following expression [25]:

$$t = \frac{\lambda_1 \lambda_2}{2(n_1 \lambda_2 - n_2 \lambda_1)} \quad (1)$$

where λ_1 λ_2 are the wavelengths at the maxima in nm whereas n_1 and n_2 are the refractive indexes at λ_1 λ_2, respectively. n_1 and n_2 are given by the following formula [25, 26]:

$$n_{1,2} = \sqrt{N_{1,2} + \sqrt{{N_{1,2}}^2 + S^2}} \quad (2)$$

and

$$N_{1,2} = \left(\frac{1+S^2}{2}\right) + 2S\left(\frac{T_{max}-T_{min}}{T_{max}T_{min}}\right) \quad (3)$$

where S the refractive indexes glass (S_{glass}=1.52),T_{max} and T_{min} represent the maxima and minima of the transmittence spectrum

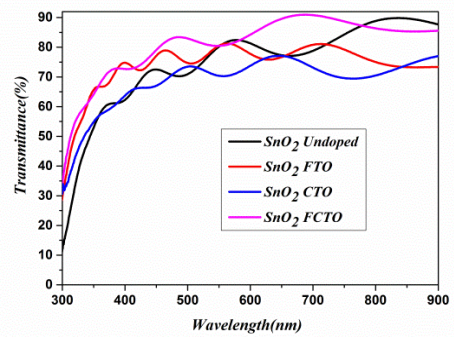

Fig. 1. Transmittance spectra of undoped, F doped SnO_2:(FTO), Co doped SnO_2:(CTO) and F-Co co-doped SnO_2: (FCTO) thin films.

The obtained thickness are ranged from 960nm to 1300nm as seen in Table 1. Based on estimated thickness values, there is an contrary relationship between transmittance value and the thickness of the layers with the respect of Beer-Lambert low.

As well known tin oxide has direct band gap (E_g), for all samples E_g was deduced from Tauc's expression [27] in respect to the following equation:

$$(\alpha h\upsilon)^2 = A(h\upsilon - E_g) \quad (4)$$

where α is the absorption coefficient and A is a constant. E_g values decrease with doping and co-doping from 3.94 to 3.77eV for undoped to Co doped tin oxide.

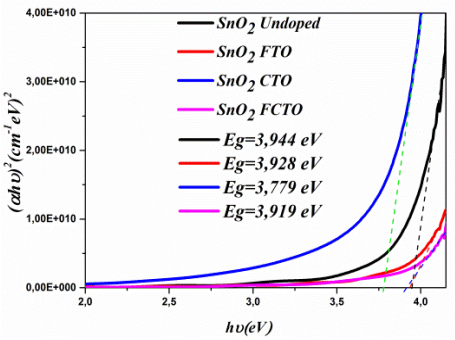

Fig. 2. Band gap (Eg) estimation from Tauc relation of undoped tin dioxide, F doped (FTO), Co doped SnO_2 (CTO) and F-Co co-doped SnO2 (FCTO) thin films.

Fig. 2 shows the band gap assessment from Tauc relation of undoped, F or Co doped, and F+Co co-doped tin dioxide. The whole changes in E_g were given in Table 1.

Table 1. Films thickness, Band gap and Transmittance values of undoped, F doped SnO_2:(FTO),

Co doped SnO_2:(CTO) and F-Co co-doped SnO2: (FCTO).

Material	*t (nm)*	*Eg(eV)*	*T(%)*	*R_{sh} ($\Omega.cm^{-2}$)*
Undoped SnO_2	1098.24	3.944	78.16	177.35
SnO_2: FTO	1136.94	3.928	77.71	20.34
SnO_2: CTO	1373.77	3.779	73.76	127.46
SnO_2: FCTO	960.36	3.919	83.73	38.56

3.2. FTIR analysis

FTIR spectra of undoped, F-doped, Co-doped and F+Co co-doped SnO_2 thin films, in 400-4500 cm^{-1} range are shown in Fig. 3. Peak at 1040 nm may be related to O-H vibration which adsorbed to the surface of the elaborated samples. The related Sn-O-Sn vibration, at peaks 773 cm^{-1}, appears in all samples which leads us to proclaim the formation of the SnO_2 product [28] in the whole samples. It was worth that for F-doped SnO_2 a F-Sn-F vibration appears at 418cm^{-1} [29-31] and subsists even in F-Co doped SnO_2.

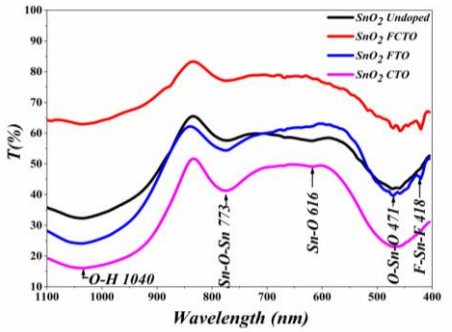

Fig. 3. FT-IR spectra of undoped, F doped SnO_2:(FTO), Co doped SnO_2:(CTO) and F-Co co-doped SnO_2: (FCTO) thin films.

For the cobalt doped samples the O-Sn-O absorption peck appears at 471cm^{-1} [28], it becomes larger with high intensity than the peak in the undoped SnO_2 sample. The effect Co doping and its presence in the Co doped sample is not well remarked.

For F-Co doping sample it is well known that each dopant Co and F enter in substations with Sn and oxygen separately but effect of F doping is still dominant because of the amount of fluorine.(F(7wt%) and Co(2.5wt%) hence the F-Sn-F vibration appearing at 418cm^{-1} subsists in F-Co doped SnO_2.

3.3. Structural properties and surface morphological analysis

3.3.1. XRD analysis

The XRD patterns for the undoped SnO_2, FTO, CTO, and FCTO layers grown on glass substrates have been studied in the 2θ range of 10-90° as can be seen in Fig. 4. X-ray diffraction show that formation of SnO_2 under rutile structure with several diffraction peaks at 2θ = 26.61, 37.95 and 51.82°along (*110*), (*200*) and (*211*) planes, respectively according to JCPDS card No:41-1445 (a_0=b_0=4.737Å,c_0=3.185Å) [32]. XRD samples spectra show that the preferred trend is (200) peak at 37.95°. Intensity of this peak increases and reaches its maximum with Co-doped SnO_2. Further the more peak at 29.9° corresponding to (*101*) plan of SnO_2 phase formation was observed only with the case of F-doping and Co-doping SnO_2 leading to an increment in SnO_2 crystallite size over 31.60nm for the considered concentration.

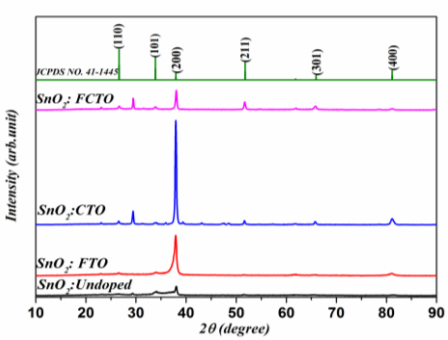

Fig. 4. XRD patterns SnO_2 images of undoped, F doped SnO_2:(FTO), Co doped SnO_2:(CTO) and F-Co co-doped SnO_2: (FCTO) thin films.

Using Scherrer's formula, the mean crystalline size (*D*) of undoped, F-doped, Co-doped and F+Co co-doped SnO_2 thin films, was calculated according to the equation below [33]:

$$D = \frac{0.9\lambda}{\beta \cos\theta} \tag{5}$$

where *D* is the crystalline size, β is the broadening of the diffraction line measured at ful width at half maximum intensity (FWHM) in (rad), and λ is the X-ray wavelength (1.5406Å). The XRD parameters, such as crystalline size (*D*) and the phases identified along with the (200) plane. Values of them were illustrated in Table. 2. It is worth noting that crystallite size increases gradually from 23.33nm for pure SnO_2 to reach 25.91nm, 31.60, and 31.61 for FTO, CTO and FCTO in this order.

Table 2. Lattice parameters a, and c, crystallite size D and R_{sh} of the products.

Material	**Lattice constants(Å)**				***D (nm)***	***R_{sh} ($\Omega.cm^{-2}$)***
	a	**$\Delta a=a-a_0$**	**c**	**$\Delta c=c-c_0$**		
Undoped SnO_2	4.7701	0.03195	3.175	-0.0121	23.33	177.35
SnO_2: FTO	4.7614	0.02329	3.173	-0.0133	25.91	20.34
SnO_2: CTO	4.7427	0.0057	3.203	0.0159	31.60	127.46
SnO_2: FCTO	4.7226	-0.0144	3.228	0.0409	31.61	38.56

For more information about the structure and growth of the layers, texture coefficients and lattice parameters were calculated according to the following formula [34]:

$$TC(hkl) = \frac{I(hkl)/I_0(hkl)}{N^{-1}\sum_n^N I(hkl)/I_0(hkl)} \tag{6}$$

and

$$\frac{1}{d_{hkl}^2} = \frac{h^2+k^2}{a^2} + \frac{l^2}{c^2} \tag{7}$$

where *I(hkl)* is the plane *(hkl)* measured relative intensity, $I_0(hkl)$is the standard intensity taken from the JCPDS data of the same plane *(hkl)*, ***N*** is the reflection number and *n* is the number of diffraction peaks. Whereas (*hkl*), d_{hkl}, '*a*' and 'c' are the miller indexes, the inter-planar distance, and the lattice constants, respectively.

A growth along <200> direction plane is the preferred orientation. As seen in the Fig. 5 the coefficient becomes more significant when SnO_2 is doped with fluorine. The calculated value *a* is greater than the value a_0 of the JCPDS card No:41-1445 ($a_0=b_0=4.737$Å,$c_0=3.185$Å) for the doping with undoped, F doped and Co doped only then becomes weaker than a_0 for the case of F+Co co-

doped layer. Whereas the parameter *c* starts weaker then becomes greater than c_0 as recapitulated in Table 2.

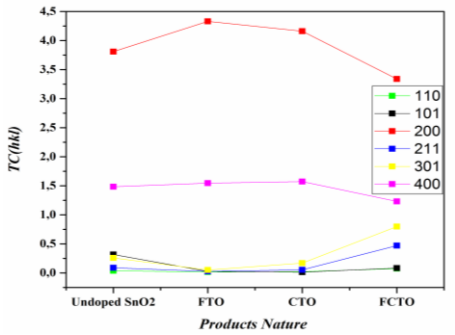

Fig. 5. TC (hkl) variation of undoped, F doped SnO_2: (FTO), Co doped SnO_2:(CTO) and F-Co co-doped SnO_2: (FCTO) thin films.

3.3.2. Surface morphologies

The films morphology is studied by SEM (Jeol model TESCAN VEGA3). Fig. 6 exhibits SEM images of the surface samples at the same magnification. As shown in Fig. 6 a) the undoped sample has homogenous surface with few agglomeration of pure SnO_2 as it was established by special EDX focus on those points (see EDX results corresponding to Fig. 6 a). For FTO sample surface, the agglomerations become as small granules in size with high density. Also by special EDX focus on those agglomerations and elsewhere (see EDX results corresponding to Fig. 6 b) it was revealed that the product structure is a compounded of Sn, O, and F with flour percentage around 6 at. %. Fig. 6 c) shows that the agglomerations become large in size with cobalt doping (CTO sample) and EDX focus reveals the percentage of Sn, O, and Co as 23.58, 73.04, and 3.38 at. %, respectively. Yet for the co-doped sample, the agglomerations become as mixture of small and large size granules. Also by special EDX focus on those agglomerations (see EDX results corresponding to Fig. 6 d), the structure of the product is a compounded of Sn, O, F and Co with the corresponding percentage of Sn, O, F, and Co around 28.00, 64.28, 6.59 and 1.14 at. % revealing the co-existence of cobalt and fluorine as doping elements substituting the tin atoms and oxygen ones, respectively.

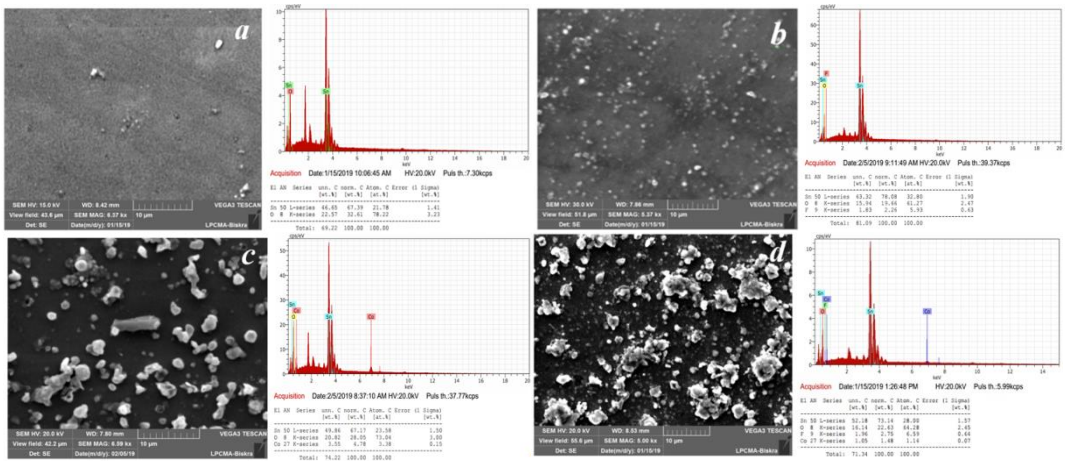

Fig. 6. SEM images and EDX of a) undoped, b) F doped SnO_2:(FTO), c) Co doped SnO_2:(CTO), and d) F-Co co-doped SnO_2: (FCTO) thin films.

3.4. Electrical properties

Sheet resistance ($\boldsymbol{R}_{sh}$) was measured with the help of four-point probe where the current (I) is applied between the outer two contacts and the potential difference (V) is measured across the inner two probes [35], A corrective factor of 4.532 is used. Sheet resistance value can be obtained from the last relation as follow:

$$R_{sh} = 4.532\left(\frac{V}{I}\right) \tag{8}$$

Table 2 gives $\boldsymbol{R}_{sh}$ values of the undoped, F-doped, Co-doped and F-Co co-doped SnO_2. As well known previously that F-doped tin oxide is a conductor [36]. Co-doped SnO_2 thin films were less conducting, at room temperature, than F-doped one but more conducting than undoped SnO_2. Either for F-Co co-doped, the film was found more conducting than Co-doped and less conducting than F-doped thin films tin oxide (For more precision see $\boldsymbol{R}_{sh}$ values in Table 3).

4. Conclusions

Undoped, FTO, CTO and FCTO thin films were deposited onto 480°C preheated glass substrates using (SPMN). The studied samples concentrations are 7 wt %, 2.5 wt %,(7 wt%+2.5wt%) co-doped SnO_2. Effect of F and Co doping and F+Co co-dopeding concentration on structural and optical properties of SnO_2 thin films were investigated. Optical transmittance spectra showed an average 73-83% and E_g values between 3.77 to 3.94eV whereas the films thicknesses varied between 960-1373nm. Structural studies using FT-IR analysis of spectra confirmed the existence of Sn-O-Sn, F-Sn-F, and O-Sn-O bonds vibrations modes in the product. Also X-ray diffraction show rutile structure formation of SnO_2. An additive peak at 29.9° corresponding to (*101*) plan of SnO phase formation was observed only with F-doping and Co-doping SnO_2 cases. Crystallite size average was 23-31nm for the considered doping SnO_2 product.

Acknowledgments

This work was supported in part by VTRS laboratory of El-Oued University. X-ray diffraction was acquired with an instrument supported by CENTRE DE DEVELOPPEMENT DES TECHNOLOGIES AVANCEES

References

[1] H. Ma, D. Zhang, S. Win, S. Li, Y. Chen, Solar energy materials and solar cells **40**(4), 371 (1996).
[2] H. Kim, A. Pique, Applied physics letters **84**(2), 218 (2004).
[3] K. Ravichandran, G. Muruganantham, B. Sakthivel, Physica B: Condensed Matter **404**(21), 4299 (2009).
[4] H. Kim, R. Auyeung, A. Piqué, Thin Solid Films **516**(15), 5052 (2008).
[5] E. Mokaripoor, M.-M. Bagheri-Mohagheghi, Materials Science in Semiconductor Processing **30**, 400 (2015).
[6] J. Szuber, G. Czempik, R. Larciprete, B. Adamowicz, Sensors and Actuators B: Chemical **70**(1-3), 177 (2000).
[7] S. Boycheva, A. K. Sytchkova, M. L. Grilli, A. Piegari, Thin Solid Films **515**(24), 8469 (2007).
[8] A. Banerjee, S. Kundoo, P. Saha, K. Chattopadhyay, Journal of Sol-Gel Science and Technology **28**(1), 105 (2003).
[9] S. Rani, S. C. Roy, N. Karar, M. Bhatnagar, Solid state communications **141**(4), 214 (2007).
[10] H.-L. Ma, X.-T. Hao, J. Ma, Y.-G. Yang, J. Huang, D.-H. Zhang, Xian-Gang Xu, Applied

surface science **191**(1-4), 313 (2002).
[11] S. Yu, W. Zhang, L. Li, D. Xu, H. Dong, Y. Jin, Applied Surface Science **286**, 417 (2013).
[12] M. Ichimura, D. Ao, Materials Science Forum **787,** 378 (2014).
[13] B. Benhaoua, S. Abbas, A. Rahal, A. Benhaoua, M. Aida, Superlattices and Microstructures **83**, 78 (2015).
[14] M.-F. Chen, K.-m. Lin, Y.-S. Ho, Materials Science and Engineering: B **176**(2), 127 (2011).
[15] S. Chandra, K. Ravichandran, G. George, T. Arun, P. Rajkumar, Journal of Materials Science: Materials in Electronics **27**(9), 9558 (2016).
[16] G. Korotcenkov, I. Boris, V. Brinzari, S. Han, B. Cho, Sensors and Actuators B: Chemical **182**, 112 (2013).
[17] Z. Bin, Y. Chenbo, Z. Zili, T. Chunmin, Y. Liu, Sensors and Actuators B: Chemical **178**, 418 (2013).
[18] E. Zampiceni, E. Bontempi, G. Sberveglieri, L. E. Depero, Thin Solid Films **418**(1), 16 (2002).
[19] G. Turgut, E. F. Keskenler, S. Aydın, E. Sönmez, S. Doğan, B. Düzgün, M. Ertuğrul., Superlattices and Microstructures **56**, 107 (2013).
[20] Z. Jiang, Z. Guo, B. Sun, Y. Jia, M. Li, J. Liu, Sensors and Actuators B: Chemical **145**(2), 667 (2010).
[21] C.-M. Wang, C.-C. Huang, J.-C. Kuo, J.-L. Huang, Surface and Coatings Technology **231**, 374 (2013).
[22] L. Francioso, A. Forleo, S. Capone, M. Epifani, A. M. Taurino, P. Siciliano, Sensors and Actuators B: Chemical **114**(2), 646 (2006).
[23] Y. Meftah, D. Bekker, B. Benhaoua, A. Rahal, A. Benhaoua, A. Hamzaoui, Digest Journal of Nanomaterials and Biostructures **13**(2), 465 (2018).
[24] J. Manifacier, J. Gasiot, and J. Fillard, Journal of Physics E: Scientific Instruments **9**(11), 1002 (1976).
[25] E. Shaaban, I. Yahia, E. El-Metwally, Acta Physica Polonica-Series A General Physics **121**(3), 628 (2012).
[26] R. Swanepoel, Journal of Physics E: Scientific Instruments **16**(12), 1214 (1983).
[27] J. Tauc, R. Grigorovici, A. Vancu, physica status solidi (b) **15**(2), 627 (1966).
[28] B. Zhang, Y. Tian, J. Zhang, W. Cai, Materials Letters **64**(24), 2707 (2010).
[29] S. Chaisitsak, Sensors **11**(7), 7127 (2011).
[30] B. Zhang, Y. Tian, J. Zhang, W. Cai, Physica B: Condensed Matter **406**(9), 1822 (2011).
[31] F. Arefi-Khonsari, N. Bauduin, F. Donsanti, J. Amouroux, Thin Solid Films **427**(1-2), 208 (2003).
[32] O. Elsherif, G. Muftah, O. Abubaker, I. Dharmadasa, Journal of Materials Science: Materials in Electronics **27**(12),12280 (2016).
[33] P. Scherrer, Kolloidchemie Ein Lehrbuch, ed: Springer, 387 (1912).
[34] P. Paufler, Kristall und Technik **16**(9), 982 (1981).
[35] A. Benhaoua, A. Rahal, B. Benhaoua, M. Jlassi, Superlattices and Microstructures **70**, 61 (2014).
[36] A. Rahal, A. Benhaoua, C. Bouzidi, B. Benhaoua, B. Gasmi, Superlattices and Microstructures **76**, 105 (2014).